Optical properties of normal and diseased human breast tissues in the visible and near infrared

Phys. Med. Biol., 1990, Vol. 35, No 9, 1317-1334. Printed in the UK

Optical properties of normal and diseased human breast tissues in the visible and near infrared

V G Peters†, D R Wyman†, M S Patterson† and G L Frank‡

† Hamilton Regional Cancer Centre and McMaster University, 711 Concession Street, Hamilton, Ontario, Canada L8V 1C3

‡ Department of Anatomic Pathology, Henderson General Hospital, 711 Concession Street, Hamilton, Ontario, Canada L8V 1C3

Received 16 February 1990, in final form 14 May 1990

Abstract. The optical absorption and scattering coefficients have been determined for specimens of normal and diseased human breast tissues over the range of wavelengths from 500 to 1100 nm. Total attenuation coefficients were measured for thin slices of tissue cut on a microtome. The diffuse reflectance and transmittance were measured for 1.0 mm thick samples of these tissues, using standard integrating sphere techniques. Monte Carlo simulations were performed to derive the scattering and absorption coefficients, as well as the mean cosine of the scattering angle. The results indicate that scatter exceeds absorption by at least two orders of magnitude. Absorption is most significant at wavelengths below 600 nm. The scattering coefficients lie in the range 30-90 mm^{-1} at 500 nm, and fall smoothly with increasing wavelength to between 10 and 50 mm^{-1} at 1100 nm. The scattering coefficient for adipose tissue differs, in that it is invariant with wavelength over this spectral range. For all tissues examined, the scattered light is highly forward peaked, with the mean cosine of the scattering angle in the range 0.945-0.985. Systematic differences between the optical properties of some tissue types are demonstrated.

1. Introduction

Studies of transillumination breast imaging have usually focused on the clinical evaluation of specific source-detector systems. Originally, the procedure consisted of the direct viewing of shadows cast by transmitted light when the breast was illuminated with an intense light beam (Cutler 1929). More recently, the use of near-infrared wavelengths has been introduced in which case images are recorded on infrared-sensitive photographic film (Ohlsson *et al* 1980) or viewed in real time using television cameras sensitive to near-infrared radiation. Some commercially available systems have the capability of presenting transmission data in two or more spectral bands (Profio *et al* 1988). Clinically, transillumination has been shown to be useful in distinguishing cystic from solid lesions and is particularly valuable in the diagnosis of haematoma. It has been able to detect some cancers which were not demonstrated by mammography (Wallberg 1985) and may, therefore, be a useful complementary procedure. However, transillumination is still an experimental technique. Although it has the advantage of being a risk-free method of evaluating breast disease, current procedures are limited in their ability to detect small, deep lesions (Bartrum and Crow 1984, Sickles 1984, Geslien *et al* 1985). The optimisation of transillumination requires a better understanding of the basic optical properties of breast tissues and the imaging process.

0031-9155/90/091317+18$03.50

Until very recently, there have been no quantitative studies of the propagation of visible and near-infrared light through breast tissues. In 1982, Carlsen suggested the possibility of a difference between the spectral attenuation of cancerous and normal breast tissues. Watmough (1982), however, was unable to demonstrate a correlation between transmittance and breast pathology. Ertefai and Profio (1985) also concluded that the transmittance of cancerous and glandular breast tissues showed little difference over the range 600–1060 nm. They did, however, observe greater transmittance for adipose tissue in the red region of the spectrum. All of these authors demonstrated increased attenuation in tissues with high blood content and speculated that the detection of tumours may be largely due to increased vascularity. Only Ertefai and Profio (1985) attempted to model the light–tissue interaction process. The absorption and scattering coefficients, which they obtained using Kubelka–Munk theory (Kortum 1969), were derived under the assumption of isotropic scattering in an infinite medium and, therefore, are not directly comparable with the fundamental interaction coefficients defined below.

In this paper, the optical properties are defined as follows: Σ_a and Σ_s represent the probabilities per unit infinitesimal pathlength that a photon will be absorbed or scattered respectively. All scattering interactions are considered to be elastic. The total attenuation coefficient, Σ_t, is the sum of Σ_a and Σ_s. The ratio of Σ_s to Σ_t is the single scattering albedo, a. We have assumed that the interaction centres are randomly oriented, so that the absorption and scattering coefficients are independent of the original photon direction. The scattering phase function, $S(\theta)$, is used to describe the angular dependence of the scattering, where θ is the angle between the incident and scattered photon directions. Although scatter phase functions may be quite complex, in this work $S(\theta)$ is represented by the Henyey–Greenstein function (Henyey and Greenstein 1941) given by

$$S(\theta) = 0.5(1-g^2)/(1+g^2-2g\cos\theta)^{3/2}. \tag{1}$$

This function has frequently been used to examine the influence of anisotropy in light scattering (van de Hulst 1980) and contains one free parameter, g, which is the mean cosine of the scattering angle. This parameter can be selected to change the shape of the function from one which is isotropic ($g=0$), to one which is sharply forward peaked ($g \to 1$). The transport coefficient, Σ_s', is a modified scattering coefficient given by $\Sigma_s(1-g)$.

This paper describes a technique which has been developed to determine the optical characteristics of tissues for wavelengths in the range 500–1100 nm. This method has been applied to the investigation of diseased and normal breast tissues. The tissues were obtained from surgical specimens and consisted of normal glandular and adipose tissues, ductal carcinoma, fibrocystic tissue and fibroadenoma. The last two are the most common benign breast conditions. Total attenuation coefficients were measured for thin slices of tissue cut on a microtome. The diffuse reflectance, R_M, and transmittance, T_M, were measured for 1.0 mm thick samples of these tissues, using standard integrating sphere techniques. Monte Carlo simulations of the integrating sphere measurements were then performed to derive the scattering and absorption coefficients. In addition, the mean cosine of the scattering angle was determined assuming that the scatter phase function for tissue can be represented by a Henyey–Greenstein function. The validity of the technique was established by experiments with suspensions of polystyrene microspheres and ink having known scattering and absorption properties.

2. The Monte Carlo model

A Monte Carlo simulation of the reflectance and transmittance measurements was performed using the geometry shown in figure 1. A parallel beam of light of diameter d is assumed to be incident normally on the sample, which is held between 1.0 mm thick glass slides. The light beam is further assumed to have a uniform intensity distribution. All light emerging through the apertures of diameter D, on the entrance and exit faces of the sample holder, is assumed to be detected. The calculated transmittance, T_C, is that fraction of the incident irradiance which emerges through the exit face of the sample holder. It includes both unattenuated photons and forward scattered photons. The calculated reflectance, R_C, is that fraction of the incident irradiance which is backscattered through the aperture on the entrance face of the sample holder. R_C does not, however, include the incident photons which are specularly reflected on first encounter with the air-glass interface. The loss at this surface was calculated as 4.0%, based on a refractive index of 1.5 for crown glass.

The input to the Monte Carlo program includes a, g and Σ_t for tissue as well as the geometric parameters d and D. The attenuation coefficient for glass was taken to be zero, as measurements showed it to be negligible in this wavelength range. Each photon history begins with the random selection of its position within the incident beam. The fraction of light reflected at glass-air interfaces is calculated using the Fresnel reflection coefficients for randomly polarised light. At tissue-glass interfaces, photons are assumed to change direction due to the mismatch in refractive index; however, specular reflections are ignored as the reflection coefficient is only about 0.4% for normal incidence. For our simulations, we assumed that the refractive index of tissue is identical to that of water (1.33).

Pathlengths in tissue are calculated using the cumulative distribution sampling method (Carter and Cashwell 1975), according to

$$l_j = -\ln |n_j| / \Sigma_t \tag{2}$$

where n_j is a randomly generated number between 0 and 1. For interactions in tissue, the scattering angle, θ, is randomly sampled from the Henyey-Greenstein function. The azimuthal angle is randomly and uniformly sampled between 0 and 2π. Survival weighting is used for each interaction as a means of variance reduction. That is, each interaction is assumed to be a scatter, with absorption accounted for by having the photon retain only a fraction of its incident weight. The scattered weight is the product of the albedo and the weight of the photon prior to the interaction. For interactions at glass-air interfaces, the Fresnel reflection coefficient replaces the albedo in this

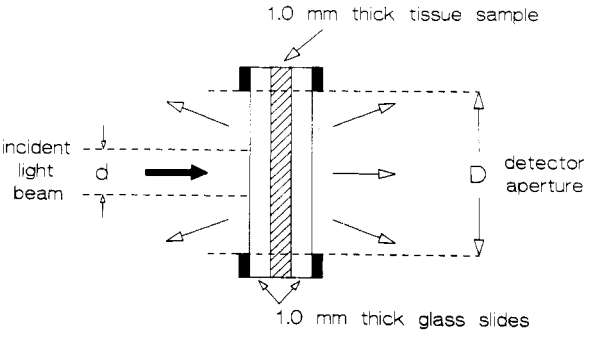

Figure 1. Geometry for the Monte Carlo simulation of reflectance and transmittance measurements.

product. The weighted fraction which crosses the glass-air interface within the limits of the detector aperture is scored as reflected or transmitted depending on the surface through which it exits. The history of the scattered fraction continues until the surviving weight falls below a value sufficiently small that roulette (Carter and Cashwell 1975) is used to determine the fate of the particle. New incident photons are selected up to a predetermined limit.

The Monte Carlo program was run for a selected set of the parameters a, g and Σ_t to generate a set of data which could then be used for interpolation of specific results. The beam diameter, d, and aperture size, D, were taken to be 3.0 and 12.7 mm to correspond with the experimental conditions. For each value of a and g, the calculated reflectance, R_C, (or transmittance, T_c) was plotted as a function of the total attenuation coefficient. Families of curves corresponding to various g values were plotted on a single graph. The complete data set consisted of graphs corresponding to a values of 1.0, 0.998, 0.995, 0.990, 0.980 and 0.960. Two of these data sets are illustrated in figures 2 and 3. For any given sample, the measured reflectance, R_M, combined with the measured attenuation coefficient, Σ_t, can be used to obtain pairs of compatible values of a and g from these graphs. Similarly, the measured transmittance, T_M, combined with Σ_t can be used to obtain a second set of acceptable pairs. The correct values of a and g are the only mutually acceptable values interpolated from the paired data sets.

Acceptable errors in the calculated reflectance and transmittance were achieved using 5000 incident photons for each Monte Carlo run. In each case the photons were

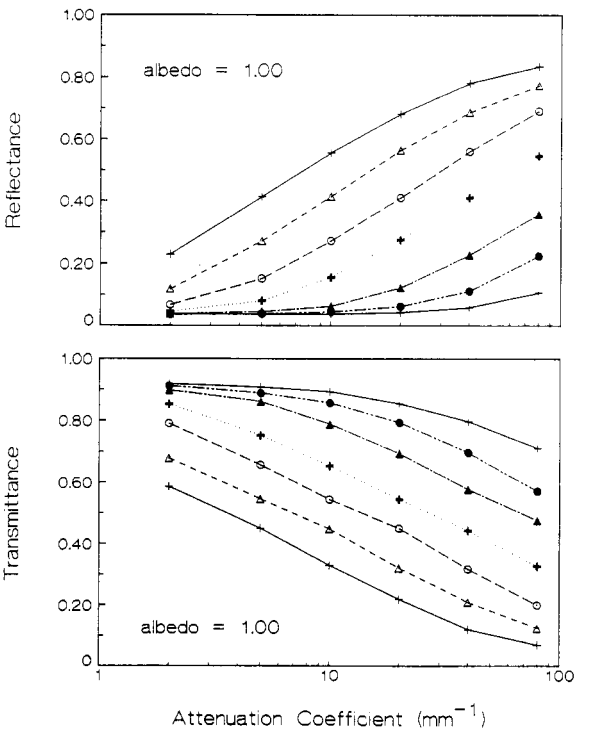

Figure 2. Reflectance and transmittance as determined from the Monte Carlo model, plotted as functions of Σ_t for a range of g values: +, 0.60; △, 0.80; ○, 0.90; ✚, 0.95; ▲, 0.98; ●, 0.99; +, 0.995. Albedo = 1.00.

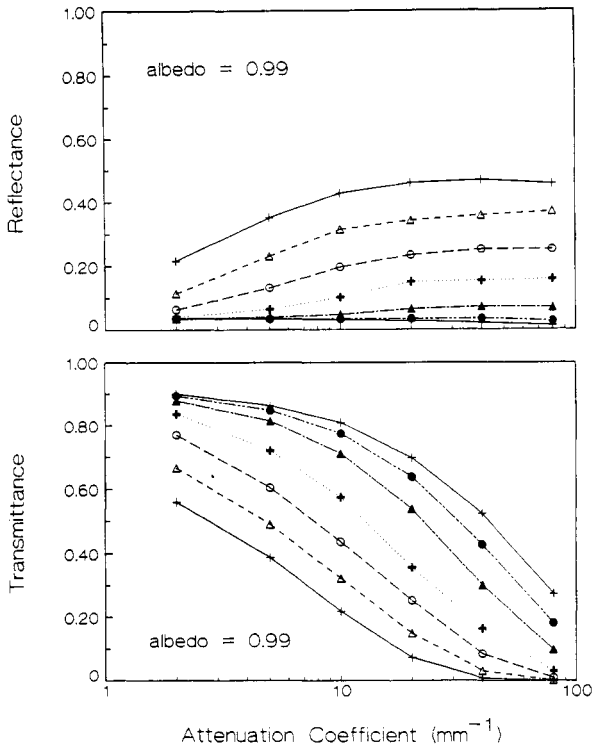

Figure 3. As figure 2, but albedo = 0.99.

divided into five groups of 1000 photons with the errors in R_C and T_C taken as the standard error in the mean of the values obtained for the five groups. The absolute errors were usually within ±0.005 and were always within ±0.01.

3. Materials and methods

3.1. Apparatus

The light source used for these experiments was a xenon arc lamp coupled with a monochromator for wavelength selection. The emergent light was collimated and then weakly focused as shown in figure 4(*a*). Focusing was necessary to maintain a high signal to noise ratio in the measurement geometry described below. A wavelength calibration of the system indicated an accuracy within 3 nm with an output bandwidth of 4 nm. A 500 nm long-pass filter was included in the beam to remove second-order diffraction lines passed through the monochromator. The optical system was enclosed in a blackened box to minimise interference by internal reflections and external light sources.

For measurement of the total attenuation coefficients, the light beam was directly incident on a collimated photodiode coupled to a preamplifier (figure 4(*b*)). The samples were positioned 30 cm in front of the photodiode and the light beam incident on the sample was collimated to a diameter of 4.0 mm. A 0.2 mm aperture was placed over the diode to reject any light scattered through angles greater than 0.02°. Photons scattered from the part of the primary beam outside the limits of this aperture may

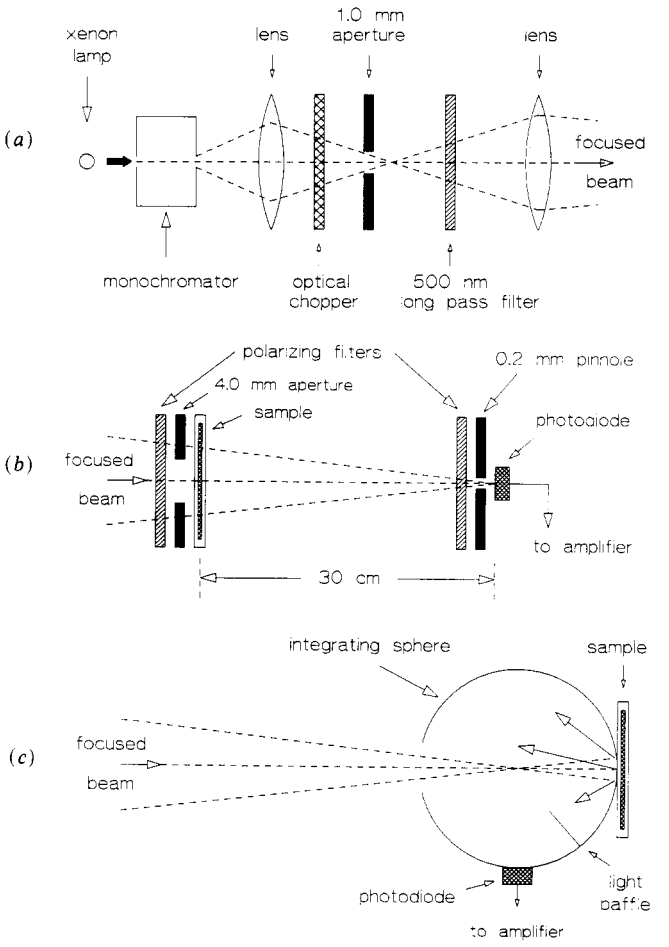

Figure 4. (*a*) The optical system used to produce a collimated, monochromatic light beam. (*b*) The experimental arrangement used to measure total attenuation coefficients. (*c*) The integrating sphere geometry used for the measurement of reflectance. For transmittance measurements the sphere was rotated 180° on a vertical axis and the open port covered with a barium sulphate reflective plate.

still contribute to the detected signal. Further scatter rejection was therefore achieved through use of a pair of polarising filters. One filter was positioned on the source side of the sample and the other placed over the detector with its polarisation axis parallel. Scattered light is preferentially attenuated by the second filter due to a change in polarisation on scattering. For optically thick specimens this technique was shown to significantly improve scatter rejection, although for the thin samples normally used for measurement of Σ_t the improvement was negligible.

For the measurement of diffuse reflectance and transmittance, a photodiode was mounted flush with the inner surface of an integrating sphere. The sphere was 10.2 cm in diameter and included two opposing beam ports, 1.27 cm in diameter. A third port, located at 90° to the other ports, was used to mount the photodiode detector. A light baffle was included between the detector port and the sample port to ensure multiple internal reflections before detection. All inner surfaces of the sphere were coated with barium sulphate. The geometry for measuring reflectance is shown in figure 4(*c*). The

centre of the sphere was positioned at the focus of the light beam emerging from the optical system. For transmittance measurements, the sphere was rotated 180° and the open port was covered with a barium sulphate reflective plate. The beam diameter was 3.0 mm at both the entrance and exit ports. This ensured that the same area of the sample was illuminated for measurement of reflectance and transmittance.

For both detector geometries, the signal from the photodiode was amplified using a lock-in amplifier. As shown in figure 4(*a*), the incident beam was modulated by a mechanical chopper which also provided a reference signal to the lock-in amplifier. Both the lock-in amplifier and the monochromator drive motor were interfaced to a computer to permit computerised data acquisition and wavelength control.

After an initial warm-up period, the xenon lamp output stayed within ±1.5%. Since the output of the lamp contains sharply peaked emission lines, resetting the monochromator can result in an additional variation of ±2.0% in the measured output at some wavelengths.

3.2. Reflectance and transmittance measurements

Using a derivation similar to that of Kortum (1969), it can be shown that for our geometry the reflectance of a sample can be approximated as

$$R = R_S(I_R/I_S) \tag{3}$$

where I_R is the reflectance measured with the sample, I_S is the reflectance measured with a barium sulphate reflective plate in the sample position and R_S is the reflectivity of the barium sulphate sphere coating. Similarly, the transmittance is given by

$$T = R_S(I_T/I_S) \tag{4}$$

where I_T is the transmittance measured for the sample.

A set of commercially available reflectance standards (Labsphere Inc., North Sutton, New Hampshire) was used to calibrate the response of the integrating sphere in reflectance measurements. The reflectivity of the sphere coating was determined by a comparison of reflectance measurements with the barium sulphate plate and the reflectance standards. The reflectivity was constant at 0.965 ± 0.01 over the entire wavelength range of interest. Using this value in equation (3), the reflectance of all the standards could be determined with a maximum absolute error of 0.03.

Freshly excised breast tissues were received from the pathology department of the Henderson General Hospital (Hamilton, Ontario) and were immediately frozen to prevent deterioration. The effects of freezing were investigated by comparing measurements with those obtained for samples which had been prepared using fresh tissues. Due to the difficulty of cutting uniform slices of 1.0 mm thickness, samples were prepared by homogenising the tissues with a scalpel. The homogenised tissues were lightly compressed between 1.0 mm thick glass slides using a 1.0 mm spacer to ensure a uniform thickness. The edges of the slides were sealed with epoxy to prevent dehydration of the sample. The validity of the homogenisation techniques was tested by comparing the results using homogenised samples with those of 1.0 mm thick slices successfully cut from the same specimen.

Reflectance and transmittance measurements were performed using the integrating sphere as already described. Automated scans were performed, with readings taken at 10 nm increments over the range 500–1100 nm. For every sample, similar measurements were made with the barium sulphate plate in the reflectance geometry. Equations (3)

and (4) were applied in the analysis of all sample results. For a sample held between glass slides, R and T correspond to the restricted definitions used for the purposes of Monte Carlo modelling. To distinguish these quantities from the actual sample reflectance and transmittance, they are denoted by R_M and T_M.

3.3. Total attenuation measurements

In principle, the measurement of the total attenuation coefficients using the experimental arrangement of figure 4(*b*) is relatively simple. The attenuation coefficient of the tissue is given by

$$\Sigma_t = -(1/t)\ln(I/I_0) \tag{5}$$

where I is the detector reading with the sample, I_0 is a reference reading with a water sample and t is the thickness of the tissue sample. The reference cuvette and tissue holders were constructed using identical glass slides and were, therefore, subject to the same specular reflection losses and absorption in glass. The thickness of the water sample was made less than 0.004 mm to minimise absorption of light in water.

Tissue samples 1.0 mm in thickness are unsuitable for the determination of attenuation coefficients since unscattered light emerging from such a thick sample is undetectable (Flock *et al* 1987). Therefore, thin frozen sections were cut using a microtome and mounted between glass slides using a small amount of water to provide better coupling by eliminating air spaces. The edges of the slides were sealed with epoxy. For each specimen, slices were cut at several thicknesses ranging between 0.004 and 0.024 mm.

For adipose tissue, it was not possible to cut thin slices using the microtome. Thicker sections were cut from frozen specimens using a scalpel, mounted between chilled glass slides, and immediately compressed to obtain a uniform thickness. Careful compression was necessary to avoid the rupture of cells and loss of cellular fluids. Several samples were prepared from each specimen, with thicknesses ranging between 0.03 and 0.20 mm. The thicknesses were determined using a micrometer and are accurate to within ±0.005 mm.

Measurements were made for each sample using the arrangement shown in figure 4(*b*). An automated scan was performed over the wavelength range 500–1100 nm. To minimise the effects of local inhomogeneities in the samples, a 4.0 mm aperture was positioned over the sample holder such that a tissue area of reasonable uniformity was exposed to the primary beam. The same aperture was subsequently used for the reference measurement with a water sample.

At each wavelength, the attenuation of the sample was calculated as $-\ln(I/I_0)$. The results for all slices taken from the same specimen were then plotted as a function of slice thickness. These points were fitted to a straight line and the attenuation coefficient determined from the slope of this line. This technique eliminates the error associated with surface scattering at the glass–tissue interfaces. A linear fit is valid provided that the detection of scattered photons is negligible.

3.4. Verification of the Monte Carlo model

A suspension of polystyrene microspheres in water was used to test the ability of the Monte Carlo analysis to derive the optical properties. These microspheres, obtained from the University of Bristol (UK), are expected to cause light scattering with negligible

absorption. The size of the spheres was 1003 ± 32 nm and their refractive index was 1.57. The scattering coefficient is dependent on both the size and concentration of spheres. Mie theory (Bohren and Huffman 1983) was used to calculate both Σ_s and g for various wavelengths.

These two optical properties were also derived using the Monte Carlo method. R_M and T_M were measured for a 1.0 mm thick suspension containing 0.95% spheres by volume. The sample was held in a glass cuvette with 1.0 mm thick walls. The same cuvette was used to measure Σ_t using varying dilutions of spheres (0.04–0.20% spheres by volume).

To test the technique for different values of Σ_a, varying amounts of india ink were added to the microsphere suspensions (maximum ink concentration of 0.1%). As indicated by other measurements, india ink is essentially a pure absorber at these wavelengths. R_M and T_M were measured for each suspension and the optical properties were derived using the Monte Carlo method. For comparison, a direct measurement of Σ_a was made using the same concentrations of ink in water. This comparison is valid since the absorption coefficient for the microspheres alone was found to be negligible. Σ_a for each suspension of ink in water was, therefore, taken to be equal to Σ_t as measured using the geometry shown in figure 4(*b*).

4. Results

4.1. Effects of tissue preparation

Homogenisation was used in the preparation of the 1.0 mm thick samples. For two tissue specimens (one carcinoma and one fibrocystic), R_M and T_M were measured for homogenised samples as well as for 1.0 mm thick cut slices. The results were in agreement within 0.03. The normal range of variations measured for different volumes of tissue within a given sample was ± 0.03. It is assumed, therefore, that homogenisation did not produce significant changes in the optical properties of the tissues examined.

To determine the effects of freezing and storage, R_M and T_M were measured for freshly prepared samples, which were subsequently frozen. At various times, the samples were thawed and the measurements repeated. For wavelengths greater than 600 nm, the results were reproducible within ± 0.02 for periods of time up to six weeks. For wavelengths of 600 nm or less, the agreement was within ± 0.05. Attenuation measurements for thin slices cut on the microtome were always made immediately after preparation since these sections deteriorated quite rapidly.

4.2. Tissue measurements

Reflectance and transmittance were measured for a total of 33 specimens from five tissue types. Figure 5(*a*) shows typical results for a sample of normal glandular tissue. All specimens showed reduced values of both R_M and T_M at wavelengths below 600 nm, indicating increased absorption of light. It should be noted that, even in the absence of absorption, $R_M + T_M$ will be less than 1.0 due to incomplete collection of the reflected and transmitted light. For some of the samples, two distinct absorption peaks could be identified at 540 and 580 nm. The positions of these peaks correspond with known absorption peaks for oxyhaemoglobin (van Assendelft 1970). Beyond 600 nm, R_M falls smoothly as the wavelength increases, while T_M increases. This behaviour was observed for all specimens although the rate of change was less pronounced for adipose tissues.

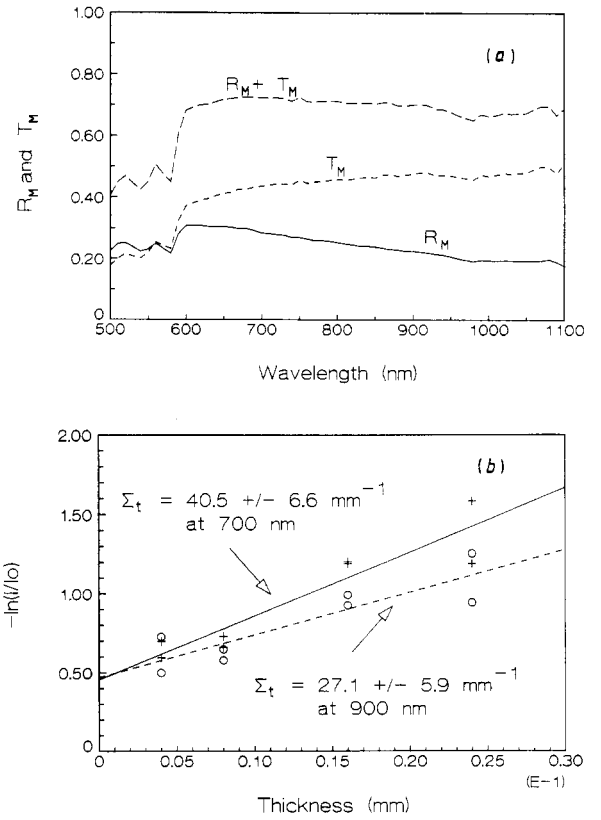

Figure 5(*a*) Measured reflectance, R_M, —— and transmittance, T_M, - - - for a sample of normal glandular breast tissue. $R_M + T_M$ is also shown ———. (*b*) Attenuation data at 700 nm (+) and 900 nm (○) for a specimen of normal glandular breast tissue plotted as a function of slice thickness. Two data points for each thickness are the result of measurements for separate samples cut from the same specimen. The slope of the fitted lines gives the attenuation coefficients.

Attenuation measurements were performed for only one specimen of each of the five tissue types due to the difficulty of making these measurements. For any given tissue slice, the measured attenuation falls smoothly as a function of increasing wavelength. At selected wavelengths, the attenuation data for each of the slices from a given specimen were plotted as a function of slice thickness. Examples of data for a specimen of normal glandular tissue are shown in figure 5(*b*) at wavelengths of 700 and 900 nm. As previously described, these points were fitted to least squares regression lines with the attenuation coefficients taken as the slope of these lines. The scatter in the data points is at least partially due to the presence of inhomogeneities in the cut slices. Extrapolation of the fitted lines to zero sample thickness indicates some attenuation which cannot be attributed to scattering in the sample. These losses account for 20–70% of the incident light, and may be caused by poor coupling of the sample with the glass slides.

4.3. Derived optical properties of tissues

Using the Monte Carlo model, the optical properties were derived for one specimen of each of the five tissue types. The results are illustrated in figure 6. The uncertainties

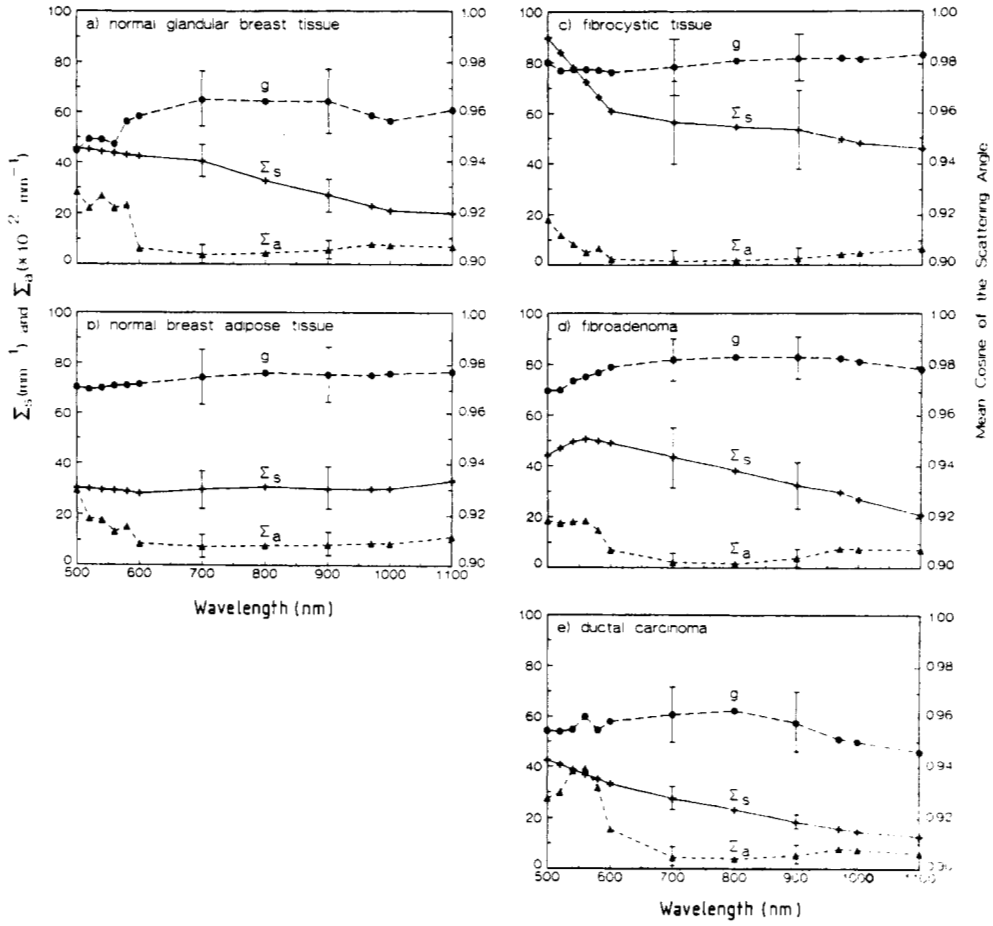

Figure 6. Derived optical properties for five tissue specimens: (*a*) normal glandular breast tissue; (*b*) normal breast adipose tissue; (*c*) fibrocystic tissue; (*d*) fibroadenoma; and (*e*) ductal carcinoma. Each data point is the result of interpolation from Monte Carlo results such as those of figures 2 and 3. Typical uncertainties are shown. (The scales on the axes are identical for all parts of the figure.)

shown were determined by the range of solutions obtainable from the Monte Carlo simulations that resulted in values of R_M and T_M within the experimental uncertainties. Errors in R_M and T_M were estimated as ± 0.03 while errors in Σ_t were taken as the standard deviation in the slope of the fitted lines.

Significant absorption is observed in all samples at wavelengths below 600 nm. In this region, carcinoma shows the greatest absorption, with a coefficient as high as 0.38 mm^{-1}. The absorption coefficient for fibrocystic tissue is lower by a factor of up to eight. For the other samples, Σ_a lies between these extremes. At wavelengths greater than 600 nm, absorption is less significant although a broad, shallow peak is observed centred at 970 nm. This coincides with the expected location of a water absorption peak (Driscoll and Vaughan 1978). Scattering coefficients exceed the absorption coefficients by at least two orders of magnitude. In general, the scattering coefficients fall as the wavelength increases. The coefficients range between 30 and 90 mm^{-1} at 500 nm and fall to between 10 and 50 mm^{-1} at 1100 nm. Adipose tissue appears to be an exception, in that Σ_s remains constant as a function of wavelength at 30 ± 6 mm^{-1}.

This result is consistent with the fact that R_M and T_M, for all the adipose tissues examined, changed little with wavelength. Although the scattering coefficients differ for each pathology, these differences are not statistically significant. The mean cosine of the scattering angle remains constant within ±0.01 for all wavelengths for any given sample. The extreme values of this quantity are 0.945 and 0.985, with no significant difference between samples.

4.4. *Analysis using similarity relations*

A unique solution for the optical properties using the Monte Carlo method depends upon the measurement of R_M, T_M and Σ_t. The principle of similarity (van de Hulst 1980) was applied to derive optical properties for the samples for which attenuation data were not available. Similarity, in this context, means that light distributions which result from the illumination of different materials will be similar provided that Σ_a and Σ_s' are matched. A knowledge of R_M and T_M should, therefore, be sufficient to estimate Σ_a and Σ_s'.

The validity of this principle was tested for our geometry using the Monte Carlo model. For fixed values of R_M and T_M, the optical properties (Σ_a and Σ_s') were derived for a range of Σ_t from 10 to 90 mm^{-1}. The results indicate that the derived absorption coefficient remains within ±0.016 mm^{-1} and the transport coefficient remains within ±8% as Σ_t is varied. These errors are smaller than those associated with the measurement of R_M and T_M.

In applying the concept of similarity to our tissue data, Σ_t was taken to be equal to the value measured for a single specimen of that tissue type. The absorption and transport coefficients were derived for each of the 33 specimens at wavelengths of 540, 700 and 900 nm. The lowest wavelength was selected to correspond with an absorption peak for haemoglobin. The data are presented in figure 7 as scattergrams of Σ_s' versus Σ_a. The mean of these values and standard deviation are provided in table 1 for each of the five tissue types.

The scattergrams demonstrate some clustering of the data points for each tissue type at each of the wavelengths considered. The points for fibrocystic and adipose tissues are particularly well clustered and separated from each other at all three wavelengths. This separation is mainly a function of the transport coefficient at 540 nm, differs along both axes at 700 nm, and is mainly a result of absorption differences at 900 nm. Σ_s' falls with increasing wavelength for fibrocystic tissue, while that for adipose tissue remains unchanged.

The data points representing carcinoma generally fall between the clusters for fibrocystic and adipose tissues with little overlap. Normal glandular tissue is similar to carcinoma at each wavelength.

Fibroadenoma exhibits a large range of absorption coefficients at all wavelengths; however, the range of transport coefficients is small.

4.5. *Results for polystyrene microspheres*

The derived optical properties for the suspension of polystyrene microspheres are presented in figure 8. The errors in the derived quantities are considerably smaller than for tissue due to the homogeneity of the samples and improved coupling at the glass–sample interface. The plotted attenuation data were well described by straight lines with the intercepts at the origin.

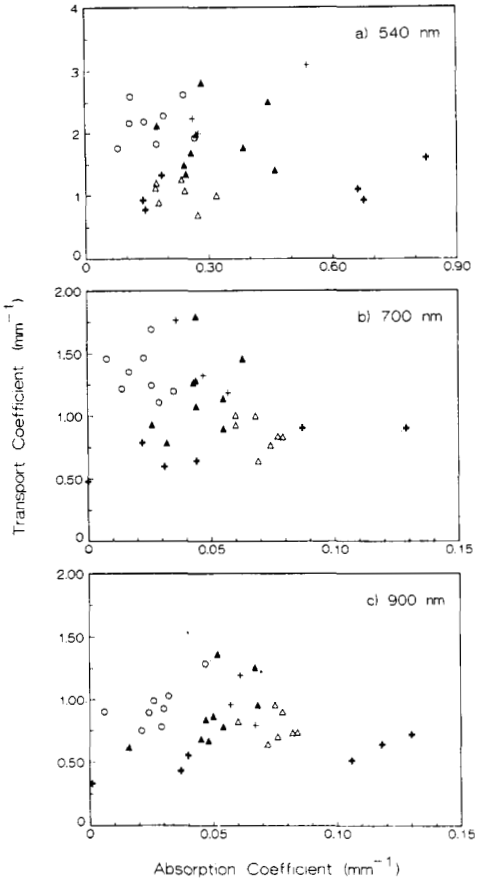

Figure 7. Scattergram of the transport, Σ_s', and absorption, Σ_a, coefficients for 33 tissue samples: +, glandular; △, adipose; ○, fibrocystic; ✚, fibroadenoma; ▲, carcinoma. Wavelengths: (*a*) 540 nm; (*b*) 700 nm; and (*c*) 900 nm.

Table 1. The mean and standard deviation of the absorption coefficient, Σ_a, and transport coefficient, Σ_s', for each of five tissue types at wavelengths of 540, 700 and 900 nm.

Tissue type[a]	540 nm		700 nm		900 nm	
	Σ_a (mm^{-1})	Σ_s' (mm^{-1})	Σ_a (mm^{-1})	Σ_s' (mm^{-1})	Σ_a (mm^{-1})	Σ_s' (mm^{-1})
Glandular (3)	0.358 ± 0.156	2.44 ± 0.58	0.047 ± 0.011	1.42 ± 0.30	0.062 ± 0.005	0.99 ± 0.20
Adipose (7)	0.227 ± 0.057	1.03 ± 0.19	0.070 ± 0.008	0.86 ± 0.13	0.075 ± 0.008	0.79 ± 0.11
Fibrocystic (8)	0.164 ± 0.066	2.17 ± 0.33	0.022 ± 0.009	1.34 ± 0.19	0.027 ± 0.011	0.95 ± 0.17
Fibroadenoma (6)	0.438 ± 0.314	1.11 ± 0.30	0.052 ± 0.047	0.72 ± 0.17	0.072 ± 0.053	0.53 ± 0.14
Carcinoma (9)	0.307 ± 0.099	1.90 ± 0.51	0.045 ± 0.012	1.18 ± 0.31	0.050 ± 0.015	0.89 ± 0.26

[a] The numbers in parentheses give the number of tissue specimens examined for each tissue type.

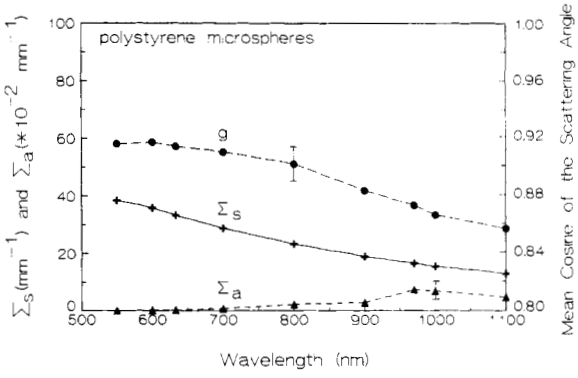

Figure 8. Derived optical properties for a suspension of polystyrene microspheres, 1003 nm in diameter (0.95% spheres by volume). The error bars for Σ_s are smaller than the symbol size.

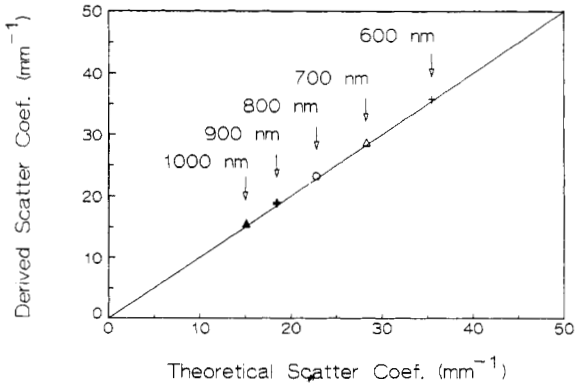

Figure 9. Comparison of the derived values of Σ_s with theoretical results at several wavelengths.

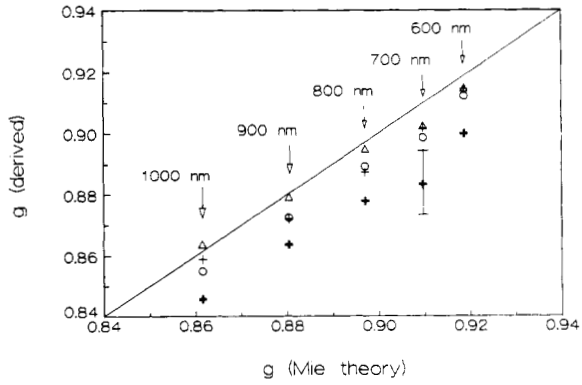

Figure 10. Comparison of the derived values of g with theoretical results at several wavelengths. The full line represents equality with the values calculated from Mie theory. The mean cosine of the scattering angle was compared for suspensions with varying amounts of ink added as an absorber (+, no ink; △, 0.006% ink; ○, 0.025% ink; ✚, 0.1% ink).

The optical properties were also calculated using Mie theory. A comparison of the scatter coefficients obtained by the two methods is presented in figure 9. The derived mean cosine of the scattering angle is compared with the theoretical value in figure 10. Each set of points in this graph corresponds to a suspension of spheres with a different concentration of added ink. These data are plotted as a function of the g values obtained from Mie theory for the spheres alone. Since ink does not contribute to light scattering, it is expected that the derived g values will be independent of ink concentration. This result is confirmed for the two suspensions having lower ink concentrations. These suspensions also demonstrate good agreement with theory. For the suspension containing 0.1% ink, however, the derived g values are significantly lower at all wavelengths. The measured and derived absorption coefficients for suspensions containing ink as an added absorber are compared in figure 11. For each ink concentration, Σ_a, as measured in water, is in good agreement with the value derived for ink mixed with polystyrene spheres. The suspension containing 0.1% ink represents an extreme case, since the absorption coefficient exceeds those determined for all tissue samples.

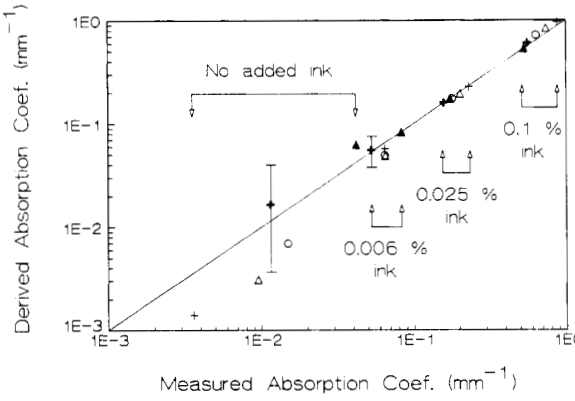

Figure 11. A comparison of the derived and measured absorption coefficients for suspensions of polystyrene microspheres with added ink. Results are presented for several wavelengths (+, 600 nm; △, 700 nm; ○, 800 nm; ✚, 900 nm; ▲, 1000 nm). For Σ_a greater than 0.1 mm^{-1}, error bars are smaller than the symbol size.

5. Discussion

The validity of the method has been demonstrated by the experiments using polystyrene microspheres and ink. Values for Σ_a, Σ_s and g agreed with those calculated or measured independently, except for a small error in g at extremely high Σ_a values. Systematic errors may have been introduced, however, through inappropriate selection of the index of refraction for tissue. Recent data (Bolin *et al* 1989) indicate that this value may lie closer to 1.40. This difference will result in errors in R_C and T_C which are usually within ±0.015 but may be as large as ±0.03. These limits were determined from Monte Carlo calculations for a range of expected values for a, g and Σ_t. These systematic errors are therefore smaller than the random errors for a given tissue sample.

The measured total attenuation coefficients for normal glandular breast tissue can be compared with values reported in the literature. In this work Σ_t was measured as 41 ± 7 mm^{-1} at 700 nm. This is in excellent agreement with the value of 40.0 mm^{-1} reported by Crilly (1986). At 635 nm, Marchesini *et al* (1989) measured an attenuation

coefficient of 39.5 mm^{-1} which also compares favourably with our value of 42 ± 7 mm^{-1}. A comparison of other properties is not possible due to the lack of published data.

Except for the absorption peaks attributed to the presence of oxyhaemoglobin and water, no significant fine structure is observed in any of the optical properties for breast tissues. The use of thicker sections for the measurement of R_M and T_M might be expected to demonstrate more subtle differences which may be significant in imaging thicker body sections such as the breast (Ertefai and Profio 1985).

Although Σ_a and Σ_s' were derived for 33 samples in this work, a derivation of the complete optical properties (Σ_a, Σ_s, g) was only performed for one sample for each pathology. In order to more accurately define the normal range of the complete properties for each pathology, it would be necessary to examine the total attenuation coefficient of a larger number of samples.

Although the optimisation of imaging procedures is beyond the scope of this work, some general comments are appropriate. For visible wavelengths, absorption by blood will greatly reduce the transmission of light through the breast; differences in tissue vascularisation will be the primary source of contrast in these images. Use of longer wavelengths will reduce the absorption of light by haemoglobin, with the result that image contrast may be less sensitive to blood concentration. Since the optical properties of fat appear to be invariant over the range of wavelengths from 700 to 900 nm, multi-wavelength imaging or subtraction imaging may be able to differentiate fat from other breast tissues. In this work we have been unable to distinguish the optical properties of ductal carcinoma from those of normal glandular breast tissues at wavelengths ranging from 500 to 1100 nm. This suggests that breast transillumination imaging might provide image contrast between these tissues only if differences in vascularity or distortion of normal structures is involved.

6. Conclusions

A technique has been developed to determine the absorption and scattering coefficients of tissues for light at wavelengths between 500 and 1100 nm. In addition, the mean cosine of the scattering angle is determined assuming that the scatter phase function can be represented by a Henyey-Greenstein function. The method is based on a combination of experimental data and a Monte Carlo model of light transport. The input parameters required for the simulation include measured values of the diffuse reflectance and transmittance of prepared samples as well as the total attenuation coefficient. The validity of the technique was established by experiments with suspensions of polystyrene microspheres and ink having known scattering and absorption properties.

This method has been applied to the investigation of diseased and normal breast tissues. The scattering coefficients were found to lie in the range 30–90 mm^{-1} at 500 nm, and fall smoothly with increasing wavelength to 10–50 mm^{-1} at 1100 nm. The scattering coefficient for adipose tissue differs from that of other tissues, remaining constant with wavelength at 30 ± 6 mm^{-1}. The mean cosine of the scattering angle for all tissue types examined lies in the range 0.945–0.985, and appears to be invariant with wavelength.

Scattering is the predominant attenuation process in tissues, with coefficients that exceed the absorption coefficients by greater than two orders of magnitude. The absorption coefficients are strongly affected by the presence of blood, particularly at wavelengths below 600 nm. Tissues of various pathologies have differing absorption coefficients and scattering properties and these differences are wavelength dependent.

Whether these differences can be exploited in transillumination imaging remains to be determined. Measurements such as those reported here will be very useful in modelling and optimising the imaging process.

Acknowledgments

The authors are grateful for the assistance provided by the technical staff of the Department of Anatomic Pathology, Henderson General Hospital. This work was financially supported by the Hamilton Civic Hospitals Research Fund and the National Cancer Institute of Canada.

Résumé

Propriétés optiques du tissu mammaire humain normal et pathologique dans le visible et le proche infrarouge.

Les auteurs ont déterminé les coefficients optiques d'absorption et de diffusion pour des échantillons de tissue mammaire humain normal et pathologique dans un domaine de longueur d'onde de 500 à 1100 nm. Ils ont mesuré les coefficients d'absorption totale pour des fines coupes de tissu coupé au moyen d'un microtome. Les réflectance et transmittance ont été mesurées pour des échantillons épais de 1 mm de ces tissues, en utilisant des techniques standards d'intégration sur une sphère. Des simulations par Monte-Carlo ont été réalisées afin d'obtenir les coefficients d'absorption et de diffusion, ainsi que le cosinus moyen de l'angle de diffusion. Les résultats indiquent que la diffusion est supérieure à l'absorption d'au moins deux ordres de grandeur. L'absorption est plus significative pour des longueurs d'onde inférieures à 600 nm. Les coefficients de diffusion se situent entre 30 et 90 mm^{-1} à 500 nm, et chutent lentement lorsque la longueur d'onde augmente pour valoir entre 10 et 50 mm^{-1} à 1100 nm. Les coefficients de diffusion pour du adipeux différent, car ils sont invariants avec la longueur d'onde pour tout ce domaine spectral. Pour tous les tissus examinés, la lumière diffusée est fortement directionnelle, avec des cosinus moyens des angles de diffusion compris entre 0,945 et 0,985. Les auteurs ont démontré l'existence de différences systématiques entre les propriétés optiques de plusieurs types de tissus.

Zusammenfassung

Optische Eigenschaften von gesundem und krankem menschlichen Brustgewebe im sichtbaren und nahen Infrarot.

Die optischen Absorptions- und Streukoeffizienten wurden bestimmt für Proben von normalem und krankem menschlichen Brustgewebe uber einen Wellenlängenbereich von 500 bis 1100 nm. Totale Schwächungskoeffizienten wurden gemessen für dünne Gewebsschnitte, die auf einem Mikrotom vorbereitet worden waren. Die diffuse Reflexion und Transmission wurde gemessen für 1.0 mm dicke Proben dieser Gewebe mit Hilfe von Standardverfahren. Monte Carlo-Simulationen wurden durchgeführt zur Herleitung sowohl der Streu- und Absorptionskoeffizieten wie auch der Streuwinkel. Die Ergebnisse weisen daraufhin, daß die Streuung die Absorption um mindestens zwei Größenordnungen übersteigt. Die Absorption ist eher von Bedeutung bei Wellenlängen unterhalb 600 nm. Die Streukoeffizienten liegen im Bereich 30-90 mm^{-1} bei 500 nm und fallen langsam mit wachsender Wellenlänge über diesen sprektralen Bereich. Für alle untersuchten Gewebe wird das Streulicht hauptsächlich vorwarts gestreut mit einem mittleren Cosinus des Streuwinkels Zwischen 0.945 und 0.985. Systematische Unterschiede zwischen den optischen Eigenschaften einiger Gewebetypen werden gezeigt.

References

van Assendelft O W 1970 *Spectrophotometry of Hemoglobin Derivatives* (Netherlands: Royal Vangorcum)

Bartrum R J and Crow H C 1984 Transillumination lightscanning to diagnose breast cancer: a feasibility study *Am. J. Roentgenol.* **142** 409-14

Bohren C F and Huffman D R 1983 *Absorption and Scattering of Light by Small Particles* (New York: Wiley)

Bolin F P, Preuss L E, Taylor R C and Ference R J 1989 Refractive index of some mammalian tissues using a fiber optic cladding method *Appl. Opt.* **28** 2297-303

Carlsen E 1982 Transillumination light scanning *Diag. Imag.* **4** 28-33

Carter L L and Cashwell E D 1975 Particle-transport simulation with the Monte Carlo method *US Energy Research and Development Administration Report*

Crilly R 1986 A study of the optical properties of soft tissue in the near infra-red *Med. Phys.* **13** 603

Cutler M 1929 Transillumination as an aid in the diagnosis of breast lesions *Surg. Gynecol. Obstet.* **48** 721-9

Driscoll W G and Vaughan W 1978 *Handbook of Optics* (New York: McGraw-Hill)

Ertefai S and Profio A E 1985 Spectral transmittance and contrast in breast diaphanography *Med. Phys.* **12** 393-400

Flock S T, Wilson B C and Patterson M S 1987 Total attenuation coefficients and scattering phase functions of tissues and phantom materials at 633 nm *Med. Phys.* **14** 835-41

Geslien G E, Fisher J R and DeLaney C 1985 Transillumination in breast cancer detection: screening failures and potential *Am. J. Roentgenol.* **144** 619-22

Henyey L G and Greenstein J L 1941 Diffuse radiation in the galaxy *Astrophys. J.* **93** 70-83

van de Hulst H C 1980 *Multiple Light Scattering Tables, Formulas and Applications* (New York: Academic)

Kortum G 1969 *Reflectance Spectroscopy—Principles, Methods, Applications* (New York: Springer)

Marchesini R, Bertoni A, Andreola S, Melloni E and Sichirollo A E 1989 Extinction and absorption coefficients and scattering phase functions of human tissues *in vivo Appl. Opt.* **28** 2318-24

Ohlsson B, Gundersen J and Nilsson D 1980 Diaphanography: a method for evaluation of the female breast *World J. Surg.* **4** 701-7

Profio A E, Navarro G A and Sartorius O W 1988 Scientific basis of breast diaphanography *Med. Phys.* **16** 60-5

Sickles E A 1984 Breast cancer detection with transillumination and mammography *Am. J. Roentgenol.* **142** 841-4

Wallberg H 1985 Diaphanography in various breast disorders *Acta Radiol. Diag.* **26** 271-6

Watmough D J 1982 Diaphanography, mechanism responsible for the images *Acta Radiol. Oncol.* **21** 11-5